Physics Letters B 838 (2023) 137704

Contents lists available at ScienceDirect

Physics Letters B

journal homepage: www.elsevier.com/locate/physletb

Large collectivity in ^{29}Ne at the boundary of the island of inversion

A. Revel [a,b,*], J. Wu [a,1], H. Iwasaki [a,c], J. Ash [a,c,2], D. Bazin [a,c], B.A. Brown [a,c], J. Chen [a], R. Elder [a,c,d], P. Farris [a,c], A. Gade [a,c], M. Grinder [a,c], N. Kobayashi [a,e], J. Li [a], B. Longfellow [a,c,3], T. Mijatović [a,f], J. Pereira [a], A. Poves [g], A. Sanchez [a,c], N. Shimizu [h], M. Spieker [a,4], Y. Utsuno [i], D. Weisshaar [a]

[a] Facility for Rare Isotope Beams, Michigan State University, East Lansing, MI 48824, USA
[b] IRFU, CEA, Université Paris-Saclay, F-91191 Gif-sur-Yvette, France
[c] Department of Physics and Astronomy, Michigan State University, East Lansing, MI 48824, USA
[d] Department of Physics and Engineering, Washington and Lee University, Lexington, VA 24450, USA
[e] Research Center for Nuclear Physics, Osaka University, Ibaraki, Osaka 567-0047, Japan
[f] Ruder Bošković Institute, HR-10002 Zagreb, Croatia
[g] Departamento de Fisica Teorica and IFT-UAM/CSIC, Universidad Autonoma de Madrid, E-28049 Madrid, Spain
[h] Center for Computational Sciences, University of Tsukuba, Tsukuba 305-8577, Japan
[i] Advanced Science Research Center, Japan Atomic Energy Agency, Tokai, Ibaraki 319-1195, Japan

ARTICLE INFO

Article history:
Received 29 July 2022
Received in revised form 10 October 2022
Accepted 16 January 2023
Available online 18 January 2023
Editor: B. Blank

Keywords:
Island of inversion
Collectivity
Inelastic scattering
Gamma spectroscopy
Transition strengths

ABSTRACT

The heavy-ion inelastic scattering of the neutron-rich nucleus ^{29}Ne to its excited states was studied using a 100.1 MeV/u ^{29}Ne rare isotope beam on ^{181}Ta and ^{9}Be targets. The combined setup consisting of the GRETINA array, the TRIPLEX device and the S800 Spectrograph facilitates the simultaneous measurements of the two inelastic reactions, providing the first measurement of the transition strengths for this isotope. A sizable E2 strength B(E2↑) which amounts to 163(30) e^2 fm^4 was determined in the excitation to the 931-keV state, demonstrating a large degree of collectivity. The present results of B(E2↑) are compared to various shell-model calculations, confirming the role of intruder configurations in ^{29}Ne at the boundary of the island of inversion.

Quadrupole collectivity is one of the fundamental collective excitation modes in atomic nuclei and known to evolve dramatically when moving away from closed shells. This behavior is robust along the valley of β stability. However, important structural changes have been observed while moving toward the region with large proton-to-neutron asymmetry [1]. In particular, the $N = 20$ magic number, arising from the separation of the $1d_{3/2}$ orbital and the $1f_{7/2}$ and $2p_{3/2}$ orbitals, disappears in neutron-rich nuclei belonging to the $N = 20$ island of inversion [2,3]. A nuclear region with pronounced deformed intruder configurations, centered around ^{32}Na, was first pointed out by the results of mass measurements suggesting extra stability of neutron-rich Ne, Na and Mg isotopes [4–8]. This was then confirmed by direct measurement of the low excitation energy of the first 2^+ excited state and the enhanced B(E2:$0^+_{gs} \rightarrow 2^+_1$) value in ^{32}Mg [9–11], providing a consistent picture of a large deformation. Later γ-ray studies suggested deformation also in neighboring isotopes such as ^{30,32}Ne [12–14], ^{31}Na [15] and ^{33,34,36,38,40}Mg [13,16–20] pointing to a large expansion of the deformation region spanning over the two major magic numbers at $N = 20$ and 28 [13,21]. As for the neutron-rich Ne isotopes, the intruder $2p_{3/2}$ assignment has been made for the ground states of ^{29,31}Ne [22,23] with a possible formation of p-wave deformed halos in ^{29,31}Ne [22–26]. It is, therefore, intriguing to examine and quantify quadrupole collectivity in odd-mass Ne isotopes, where the onset of deformation has been suggested from the sudden drop of the E(2^+) energies observed in the neighboring even-even Ne isotopes between $N = 16$ and $N = 20$ (E(2^+)=2.0 MeV for ^{26}Ne, 1.3 MeV for ^{28}Ne and 0.79 MeV for ^{30}Ne [12]).

* Corresponding author at: IRFU, CEA, Université Paris-Saclay, F-91191 Gif-sur-Yvette, France.
E-mail address: aldric.revel@cea.fr (A. Revel).

[1] Present address: National Nuclear Data Center, Brookhaven National Laboratory, Upton, NY 11973, USA.
[2] Present address: TRIUMF, Vancouver, BC V6T 2A3, Canada.
[3] Present address: Lawrence Livermore National Laboratory, 7000 East Ave., Livermore, CA 94550, USA.
[4] Present address: Department of Physics, Florida State University, Tallahassee, FL 32306, USA.

https://doi.org/10.1016/j.physletb.2023.137704

A sudden reduction of the $N = 20$ gap can also be tracked along the $N = 19$ isotones from the evolution of the energies of the lowest $7/2^-$ and $3/2^-$ states. In ^{33}Si [27], the lowest $7/2^-$ and $3/2^-$ states are located at 1435 keV and 1981 keV, respectively, above the $3/2^+$ ground state, indicative of a sizable gap at $N = 20$ between the *sd* and *fp* shells. Moving further toward the neutron-rich side, the lowest $7/2^-$ and $3/2^-$ states are observed in ^{31}Mg at much lower excitation energies of 461 keV and 222 keV [28], respectively. In addition to the migration of the negative-parity states in ^{31}Mg at low excitation energies, we observe a reordering of the lowest $7/2^-$ and $3/2^-$ states, presenting the drastic evolution of the shell structure associated with $2p_{3/2}$ orbital along the $N = 19$ line [28].

The ^{29}Ne isotope, being the last bound $N = 19$ isotone and with a neutron separation energy of 960(140) keV [29], provides a particularly attractive testing ground in order to investigate the interplay between shell evolution, deformation and possible effects from the proximity to the continuum. One-neutron removal studies from ^{29}Ne suggested J^π=$3/2^-$ for its ground state dominated by a ^{28}Ne$(0^+)\otimes 2p_{3/2}$ neutron intruder configuration and therefore placing ^{29}Ne within the island of inversion [22]. In addition, the decay of three bound excited states to the ground state of ^{29}Ne have been observed at 232(6) keV, 622(4) keV and 931(8) keV, respectively [29–31]. In the study by Liu et al. [29], where ^{29}Ne was populated via single neutron removal from ^{30}Ne, spin-parity assignments of $1/2^+$ and $3/2^-$ were tentatively proposed for the 232-keV and 622-keV excited states, respectively, although the *p*-wave nature and, hence, the $(1/2^-,3/2^-)$ assignment was not completely excluded for the 232-keV state. For the 931-keV excited state, which was weakly populated in this reaction [29], the orbital angular momenta ℓ=1, 2 or 3 were assigned and therefore the spin-parity assignment remains unknown.

In order to understand the structural evolution occurring at the boundary of the island of inversion and study quadrupole collectivity associated with intruder configurations, we performed heavy-ion inelastic scattering of the neutron-rich ^{29}Ne at intermediate energies, providing the first measurement of B(E2↑) strengths for this isotope.

In the present study, we employed two targets, ^{181}Ta and ^{9}Be, which have different atomic numbers (Z). Excitation cross sections with the high-Z (^{181}Ta) target are expected to be dominated by Coulomb excitation, whereas nuclear excitations may not be negligible at intermediate energies. On the other hand, the measurement with the low-Z (^{9}Be) target is governed by nuclear excitations. The combination of the two target measurements, therefore, allows us to probe and determine the relative importance of Coulomb and nuclear excitations to each excited state. In case of an E2 excitation, appreciable excitation cross sections are expected in both targets [32], which also provides constraints on possible spin-parity assignments for the observed states.

In the present work, the B(E2↑) value for the 931-keV excitation is obtained from its excitation cross sections with a ^{181}Ta target, whereas measurements with a ^{9}Be target are used to quantify contributions due to nuclear excitation. The transition strengths are also studied for the direct excitation to the 232-keV and 622-keV states. Inelastic scattering with the same two targets was also performed for ^{32}Mg as a reference and our results of B(E2:$0^+ \rightarrow 2^+$) for ^{32}Mg are also reported. As discussed below, an advanced Doppler-shift technique was applied using the setup consisting of the Gamma-Ray Energy Tracking In-beam Nuclear Array (GRETINA) [33,34], the TRIple PLunger for EXotic beams (TRIPLEX) [35], and the S800 spectrograph [36] in order to measure the two inelastic reactions simultaneously.

The experiment was performed at the National Superconducting Cyclotron Laboratory (NSCL) at Michigan State University. A 140 MeV/u ^{48}Ca primary beam was impinged on a ^{9}Be production target. A 100.1 MeV/u secondary ^{29}Ne beam was produced and selected by the A1900 fragment separator [37], with a purity of 25% and a typical intensity of 60 pps, before being sent to the reaction target. Reaction products were identified event-by-event by time-of-flight and energy-loss measurements from the S800 spectrograph [36,38]. Together with ^{29}Ne, a secondary beam of ^{32}Mg at 117.4 MeV/u was also produced as part of the secondary cocktail beam with a purity of 25% and a typical intensity of 60 pps.

The TRIPLEX device [35] was used in order to hold simultaneously 370 mg/cm^2 thick ^{9}Be and 2158 mg/cm^2 thick ^{181}Ta targets separated by 25 mm, the latter being placed downstream at the usual first degrader location. At the center of the Be target, the average beam energies were 96 MeV/u for ^{29}Ne and 113 MeV/u for ^{32}Mg, respectively. For the Ta target, the respective average energies were 77 MeV/u (^{29}Ne) and 90 MeV/u (^{32}Mg). The two-target foil configuration with the large foil separation allows us to identify inelastic events associated with each of the targets separately [39], as short-lived excited states produced in the ^{9}Be reaction target are expected to decay before reaching the subsequent ^{181}Ta foil.

Gamma rays emitted in-flight were detected using GRETINA [33,34], which consisted of 11 modules at the time of the experiment. GRETINA was arranged with four modules located at 58° and seven at 90° relative to the beam axis in order to maximize the coverage of the forward hemisphere. Each GRETINA module is made of four 36-fold segmented high-purity Ge detectors. A signal decomposition is performed to provide precise position information for the gamma-ray interaction points which is critical for the proper correction of the Doppler-shift effects for gamma rays emitted from ions in flight. The TRIPLEX plunger device was located about 13 cm upstream of the center of GRETINA in order to facilitate the clear identification of the Be and Ta reaction contributions using two Doppler-shifted peaks, each corresponding to inelastic events occurring in either the Be or Ta target. Similar to recoil-distance lifetime measurements [35], the clear separation of the two peaks is achieved by the combined effects of the different recoil velocities and the gamma-ray emission angles between the two targets. When the Doppler-shift correction is optimized for decay components for the ^{9}Be target (fast components), gamma rays associated with decays behind the ^{181}Ta target (slow components) are lower in energy in the Doppler-corrected spectra, due to an over-corrected velocity and under-corrected gamma-ray detection angle. This technique enables us to measure the intermediate-energy heavy-ion inelastic scattering on the Be and Ta targets simultaneously.

The Doppler-corrected gamma-ray energy spectra measured in coincidence with the inelastically scattered ^{29}Ne are presented in Fig. 1. In Fig. 1 (a), the Doppler-shift correction is optimized for the fast component (corresponding to the Be target). Therefore, peaks originating from reactions in the Be target should appear at the correct gamma-ray energies while peaks at lower energies originate from reactions occurring in the Ta target. In an analogous way, Fig. 1 (b) shows the Doppler-corrected energy spectrum when the Doppler-shift correction is optimized for the slow component (Ta target), resulting in peaks seen at the correct energies for gamma-ray events originating from the Ta target. The peak associated with reactions in the Be target is displaced to a higher energy in Fig. 1 (b). Excitation of ^{29}Ne to its 232-keV and 931-keV excited states is observed in both targets as we can clearly distinguish two Doppler-shift components, corresponding to the ^{29}Ne+Be and ^{29}Ne+Ta contributions. The appreciable yields observed for the 931-keV state with both targets suggest an E2 excitation, as discussed in Ref. [32]. The two-dimensional spectrum, displaying the gamma-ray emission angle as a function of the Doppler-corrected energy, shown in the inset of Fig. 1 (b), demonstrates that the two reaction components can be clearly separated in the present setup.

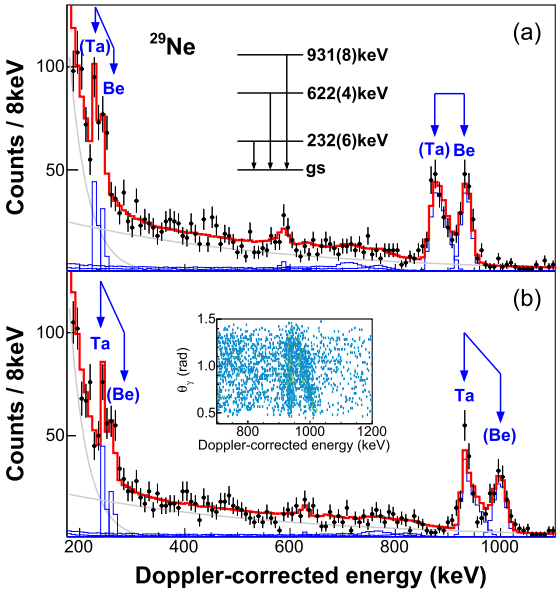

Fig. 1. Doppler-corrected gamma-ray energy spectrum, with laboratory gamma-ray angles taken below 50° (0.87 rad), obtained in coincidence with inelastically scattered ^{29}Ne when the Doppler-shift correction is optimized for a) the fast component, corresponding to the Be target and b) the slow component corresponding to the Ta target. The data are shown with black dots and error bars. The double exponential background is represented in gray while the contribution from ^{29}Ne+Be and ^{29}Ne+Ta obtained from the GEANT4 simulation are shown in blue. The sum of those three components is shown as the red solid line. In addition, the level scheme of ^{29}Ne and the two-dimensional spectrum displaying the gamma-ray emission angle as a function of the Doppler-corrected energy, are shown in the inset of (a) and (b), respectively.

In contrast to the previous results obtained with nucleon-removal reactions [29,31], the population for the 622-keV excited state is found to be very weak in the present reaction. We, therefore, focus our study on the 931-keV excited state. In order to extract full-energy-peak yields, experimental data were analyzed by a fit using the result of a GEANT4 simulation [25,40], that includes all the details of the experimental setup on top of a double exponential background. As shown in Fig. 1, the energies of 232-keV, 622-keV and 931 keV obtained in the previous work [31] (see the inset of Fig. 1 (a)) were found to reproduce the data well.

The cross sections integrated for $\theta^{lab}_{scat} \leq 2°$, where θ^{lab}_{scat} is the laboratory frame scattering angle, for the 931-keV state were measured to be 7(1) mb and 32(3) mb for the Be and Ta targets, respectively. For the 232-keV state, results of 2(1) mb and 8(2) mb were obtained for the Be and Ta targets, respectively. The quoted errors include the statistical ones, uncertainties in the fit, as well as ambiguities in the determination of the S800 acceptance and of the absolute efficiency for GRETINA. These contributions are added in quadrature. Due to the close proximity of the neutron separation energy, S_n=960(140) keV [29], no feeding from potential unobserved higher-lying states is considered in this analysis.

To extract B(E2↑) values, the measured cross sections are compared to calculations with the coupled-channel code FRESCO [41,42] following the approach described in Ref. [42,43]. The experimental scattering-angle resolution and the angular straggling were folded into the calculations before the comparison was made. Because no optical potential based on elastic scattering data is available for the present reaction, we used a theoretically derived global optical potential taken from Ref. [44] which is based on a complex G-matrix interaction, CEG07 [45,46]. Since the availability of this potential is limited to even-even nuclei and to a range of mass number from 12 to 208 [44], we derived the ^{28}Ne+^{181}Ta and ^{28}Ne+^{12}C optical potentials in order to analyze data from the ^{29}Ne +^{181}Ta and ^{29}Ne +^{9}Be scatterings, respectively. The FRESCO calculation includes two parameters, the reduced matrix element $M(E\lambda)$ which is directly related to the transition strength as $B(E\lambda; J_i \rightarrow J_f) = M(E\lambda)^2/(2J_i+1)$, and the nuclear deformation length δ_N. From the inelastic scattering cross section on the Be target, we obtain a nuclear deformation length of δ_N=1.34(11) fm for the 931-keV excitation. From the measured cross section on the Ta target we obtain B(E2↑)=148(23) e^2 fm^4 for the excitation from the ground state to the 931-keV excited state after taking the same nuclear deformation length obtained from the Be target.

In order to investigate a possible dependence on the choice of the optical potential, similar analysis was performed using a different set of optical potential parameters determined by ^{17}O+^{208}Pb scattering at 84 MeV/u [47]. Using this optical potential, δ_N=1.63(13) fm is extracted from the scattering on the Be target, and B(E2↑)=177(20) e^2 fm^4 is obtained from the Ta target. The results obtained using the above two potentials are in good agreement, although we note that the optical potential dependence is not negligible. Therefore, we took the average of the two values above and determined B(E2↑)=163(30) e^2 fm^4, where the quoted errors include experimental uncertainties and theoretical ambiguities arising from the choice of optical potentials. Our data exclude the E1 possibility for the 931-keV excitation since the expected cross section with a light target is of a few millibarn or less [48]. As for the 232-keV state which was tentatively assigned J^π=1/2$^+$ in Ref. [29], the excitation would correspond to an E1 transition. The E1 Coulomb excitation cross section with the Ta target was estimated by subtracting the cross section with the Be target after scaling with a geometrical factor Γ=2.13(45) as used in Ref. [22,49] for the Pb/C target combination. A marginal Coulomb excitation cross section of 4(3) mb is derived, leading to a B(E1↑) of 4(3)$\times 10^{-3}$ e^2 fm^2. On the other hand, the Be/Ta cross section ratio observed for the 232-keV state is very similar to that for the 931-keV excitation. Therefore, an E2 excitation is not fully excluded by the present data only, and the same analysis approach used for the 931-keV excitation results in B(E2↑) of 37(19) e^2 fm^4 for the 232-keV excitation. Note, that we could determine an upper limit of 200 ps for the decay lifetime and, hence, that the decay is governed by a faster transition such as E1 and M1, since a pure E2 decay at 232 keV results in a long lifetime on the order of 10 ns or more. For the 622-keV excitation, only a hint for the slow component was observed in Fig. 1. Therefore, only upper limits of B(E1↑)=6$\times 10^{-3}$ e^2 fm^2 and B(E2↑) = 21 e^2 fm^4 were placed. In the simulation shown in Fig. 1, an E2 excitation was considered following the (3/2$^-$) assignment made in Ref. [29]. For the 622-keV state, we assumed the same target dependence as observed for the 232-keV and 931-keV excitations, as well as a relatively long lifetime, resulting in a single peak structure corresponding to the slow component. Note that other excitation or decay scenarios are not excluded for the 622-keV state due to the limited statistic available in the present study.

In order to check the consistency of the present measurement with previous work on the well studied ^{32}Mg [11,18,50–55], we performed the same analysis for the intermediate-energy heavy-ion inelastic scattering of ^{32}Mg to its 2^+_1 excited state using the same experimental setup with the aforementioned ^{32}Mg secondary beam component. The Doppler-corrected gamma-ray spectra observed in coincidence with scattered ^{32}Mg are presented in Fig. 2. A two-peak structure associated with the Be and Ta inelastic events is clearly observed for the 2$^+$ decay. Angle-integrated cross sections with $\theta^{lab}_{scat} \leq 2°$ of 15(2) mb and 75(8) mb were extracted for the Be and Ta targets, respectively. These were obtained assuming 14(3)% feeding to the 2^+_1 state of ^{32}Mg from states between 2 and 5 MeV as determined in the previous analysis by K. Li et al. [54]. A B(E2↑) value of 380(67) e^2 fm^4 is obtained using the theoretically derived ^{32}Mg+^{181}Ta potential [44] while incorporating nuclear contributions estimated with ^{9}Be data. The

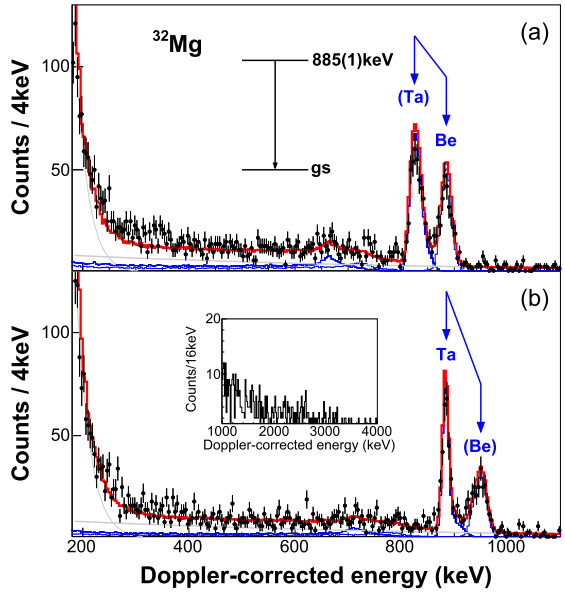

Fig. 2. Doppler-corrected gamma-ray energy spectrum, with laboratory gamma-ray angles taken below 50° (0.87 rad), obtained in coincidence with inelastically scattered ^{32}Mg when the Doppler-shift correction is optimized for a) the fast component, corresponding to the Be target and b) the slow component corresponding to the Ta target. The data are shown with black dots and error bars. The exponential background is represented in gray while the contribution from ^{32}Mg +Be and ^{32}Mg +Ta obtained from the GEANT4 simulation are shown in blue. The sum of those three components is shown as the red solid line. In addition, the partial level scheme of ^{32}Mg and the Doppler-corrected gamma-ray energy measured between 1 and 4 MeV, are shown in the inset of (a) and (b), respectively.

use of the ^{17}O+^{208}Pb optical potential results in a B(E2↑) value of 440(58) e^2 fm^4, being more consistent with the previous result obtained in Ref. [11] with the same potential. In the present study, we adopt an average value of 410(75) e^2 fm^4, where the quoted error includes experimental ones as well as the ambiguity due to the choice of the optical potential. This result is in good agreement with the value of B(E2↑)=395(30) e^2 fm^4 obtained using model-independent lifetime measurements [55] as well as with the previous adopted value of B(E2↑)=455(65) e^2 fm^4 [56], validating our analysis method.

We observed in our study that the 931-keV excited state of ^{29}Ne is strongly populated via E2 excitation. Possible J^π for this state are therefore $1/2^-$, $3/2^-$, $5/2^-$ or $7/2^-$, given that the ground state of ^{29}Ne has been assigned as $3/2^-$ [22]. In Fig. 3 (a,b,c), the experimental energy levels of ^{29}Ne are compared to the lowest negative parity states predicted from different shell-model calculations using FSU [57,58] and SDPF-M [59] interactions. The latter interactions demonstrated a good description of even-even O, Ne, Mg and Si isotopes. The FSU interaction, which was built by fitting a wide range of experimentally observed states of the *sd*-shell nuclei, was found to reproduce well the inversion of configurations observed in nuclei belonging to the island of inversion. Both the FSU and SDPF-M interactions predict the J^π=$3/2^+$ value for the ^{29}Ne ground state while the first $3/2^-$ state is located at 500 keV and 73 keV above, respectively. Focusing on the negative parity states, we observe that although both calculations agree on the ordering of the lowest $3/2^-$ and $7/2^-$ states, the energy gap between those two states goes from 871 keV using the FSU interaction to only 52 keV using the SDPF-M interaction. As noted before in ^{27}Ne [60], such a low $7/2^-$ state in the SDPF-M calculations may not be supported for ^{29}Ne, since no f-orbital contribution was observed at low excitation energies of 232 keV and below [29]. As for the 931-keV state, the assignment of $1/2^-$ and $3/2^-$ states is unlikely because both theoretical calculations predict these states to occur at higher excitation energies. The second $3/2^-$ state is predicted at

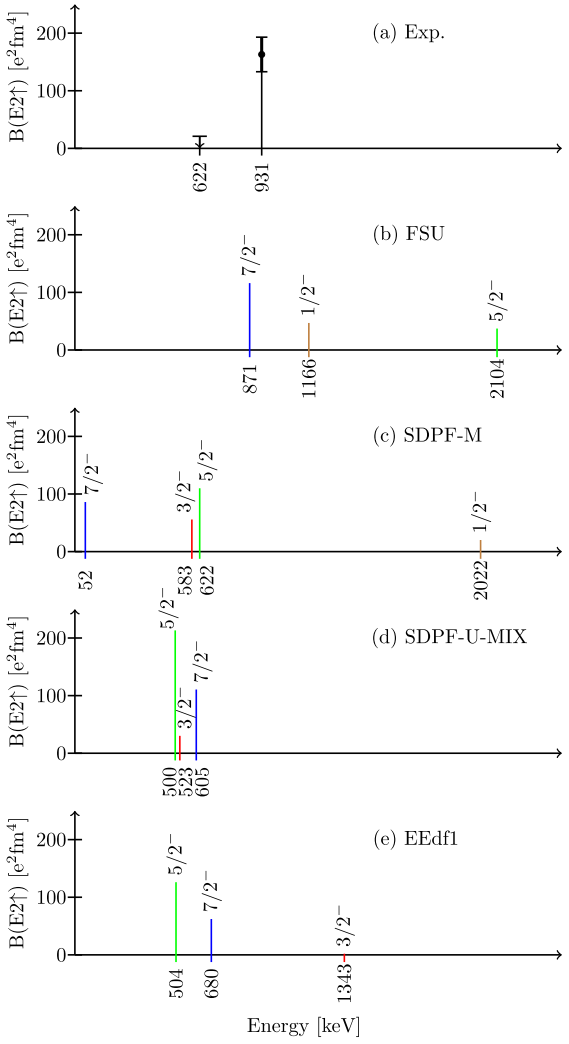

Fig. 3. Comparison of the B(E2;$3/2^- \rightarrow J^\pi$) experimental values obtained for the excited states of ^{29}Ne observed in this experiment (a) with the results from shell-model calculations using (b) FSU, (c) SDPF-M, (d) SDPF-U-MIX and (e) EEdf1 interactions. For FSU and SDPF-M calculations, a $3/2^+$ ground state is predicted and the lowest $3/2^-$ state is located at 500 keV and 73 keV, respectively. Therefore the results for (b) and (c) are plotted using the energy differences from the lowest $3/2^-$ state.

583 keV above the first $3/2^-$ using the SDPF-M interaction while no $3/2^-$ state other than the lowest-energy state is obtained below 2 MeV using the FSU interaction. Previous work tentatively identified the 622-keV state as the $3/2^-_2$ state of ^{29}Ne [29], which if confirmed, would make a J^π=$3/2^-$ assignment of the 931-keV state unlikely as the $3/2^-_3$ excited state is predicted at 2.040 MeV (1.968 MeV above the first $3/2^-$ state) by the SDPF-M calculations. In both calculations, the first $1/2^-$ excited state is predicted to be unbound at energies of 1.666 and 2.095 MeV (1.166 and 2.022 MeV above the first $3/2^-$ state), respectively. Therefore, for the 931-keV state, the $5/2^-$ or $7/2^-$ assignment remains as a plausible candidate. However, the large differences in the predicted $5/2^-$ and $7/2^-$ energies between these two calculations do not allow for further assignments.

In Fig. 3 (b,c), B(E2↑) values for the lowest negative-parity states are also plotted for the FSU and SDPF-M calculations. The effective charges used in FSU and SDPF-M calculations are proton(neutron) effective charges of 1.36e(0.45e) [57] and 1.3e(0.5e) [59], respectively. The consistency between the present 931-keV data and the $7/2^-$ state prediction given by FSU may look reasonable, whereas the lack of other low-energy negative parity states

in the calculations indicates the importance of higher particle-hole excitations in ^{29}Ne, since FSU calculations deal with only 1p2h configurations for the negative parity states. The SDPF-M calculations, which are performed with unrestricted particle hole excitations, predict several negative parity states below the threshold. However, the B(E2) strengths are rather evenly distributed among these states, at odds with the present observation.

In pursuit of a more consistent description of the B(E2) distribution in the low-lying states of ^{29}Ne, we present in Fig. 3 (d,e) the results from calculations using the SDPF-U-MIX [21] and EEdf1 [61] interactions recently developed for the sd+pf model space, both providing a good description of the nuclei at or around the island of inversion. The SDPF-U-MIX interaction is built as an extension of the SDPF-U interaction [62] allowing the mixing of different *npnh* configurations. The EEdf1 interaction was derived for the *sd-pf* shells from fundamental principles while explicitly including three-body forces and was able to reproduce nicely the energies and the E2 properties of low-lying states in neutron-rich Ne, Mg and Si isotopes [61]. The SDPF-U-MIX and EEdf1 calculations are using proton(neutron) effective charges of $1.31e(0.46e)$ and $1.25e(0.25e)$, respectively. The results obtained using the SDPF-U-MIX and EEdf1 interactions, reported in Fig. 3 (d,e), are overall consistent. The lowest $3/2^-$ state is given as the ground state in both cases, and the first $5/2^-$ and $7/2^-$ excited states are predicted at around 500 keV and 650 keV, respectively, in proximity to the presently observed 931-keV state. In addition, a $3/2^-$ excited state is predicted by the SDPF-U-MIX interaction close in energy (523 keV) to the 622-keV ($3/2^-$) state. Moreover, EEdf1 and SDPF-U-MIX results both predict the $5/2^-$ excited state to have the highest B(E2↑), with values of 126 e^2 fm^4 and 213 e^2 fm^4, respectively, which are both compatible with the experimental value of 163(30) e^2 fm^4 obtained for the 931-keV state. We also note that the recent study of neutron-unbound resonances in ^{29}Ne confirms the significant ℓ=3 components for the low-lying resonance at an excitation energy of 1.48 MeV [63]. If the $7/2^-$ spin for this state is confirmed, the $7/2^-$ assignment for the 931-keV state may be unlikely. Our experimental results point to a large enhancement of the observed B(E2↑) value for the 931-keV excited state of ^{29}Ne, which is supported by the SDPF-U-MIX and EEdf1 interactions, as E2 strengths are more localized at low excitation energies below the threshold. In Fig. 3, it is interesting to note the large decrease of the $5/2^-$ energy in the SDPF-U-MIX and EEdf1 calculations, with respect to the FSU calculations which present the $5/2^-$ state with the 1p2h configuration. The lowered $5/2^-$ energy and the resultant order of the lowest $3/2^-$, $5/2^-$ and $7/2^-$ states can be considered as a trend toward a collective $K^\pi=3/2^-$ band, making a marked contrast to the 1p2h $K^\pi=1/2^-$ band structure suggested for the low-lying negative parity states in the N=19 isotone ^{31}Mg [64]. In fact, the SDPF-U-MIX calculations provide dominant 3p4h configurations for the lowest $3/2^-$ (86%), $5/2^-$ (97%) and $7/2^-$ (56%) states, respectively. The spectroscopic quadrupole moments are given as 11 efm^2 ($3/2^-$), -5 efm^2 ($5/2^-$), and -14 efm^2 ($7/2^-$), respectively, corresponding to the intrinsic quadrupole moments of 50-70 efm^2 if one can assume the K=3/2 band. Very similar results are obtained in the EEdf1 calculations, showing the dominant (≈80%) 3p4h configurations for the low-lying negative parity states with the intrinsic quadrupole moments of 40-50 efm^2. This indicates the important role of the intruder configurations involving the 3p4h configurations in driving quadrupole deformation of ^{29}Ne.

The large degree of collectivity for the ^{29}Ne low-lying states associated with the intruder configurations can be further assessed by referring to the Nilsson diagram. Based on the measured B(E2) value, the deformation parameter β_C can be calculated using the relation $|\beta_C| = 4\pi\sqrt{B(E2\uparrow)}/(3ZeR^2\ |\langle I_i K20|I_f K\rangle|)$ with $R = 1.2A^{1/3}$ fm. Based on the K=3/2 rotational band built on the ^{29}Ne ground state, β_C is given 0.55(6) and 0.74(7) assuming $5/2^-$ and $7/2^-$ assignment for the 931-keV state, respectively. From the Nilsson diagram presented in Figure 7 of Ref. [22], one can observe that the [321 3/2] orbital, which corresponds to the neutron 3p4h configuration that is suggested by the shell model calculations for the ^{29}Ne ground state, is favored at large deformation ($0.58 < \beta < 0.8$). This alternative view provides a consistent picture of the large deformation of ^{29}Ne induced by the intruder configurations across the N=20 shell gap.

In summary, we demonstrated a modified approach of the recoil-distance Doppler-shift technique to study intermediate-energy heavy-ion inelastic scattering of ^{29}Ne on the ^{9}Be and ^{181}Ta targets at the same time. From the measured cross sections, a sizable B(E2↑) of 163(30) e^2 fm^4 was extracted for the excitation to the 931-keV excited state of ^{29}Ne. This value suggests a large enhancement in quadrupole collectivity at low excitation energies of ^{29}Ne and, hence, places this isotope in the deformed region of the island of inversion. In addition, the 232-keV and 622-keV excited states of ^{29}Ne were studied and marginal transition strengths were extracted for their excitation. The experimental data are compared to various shell model calculations developed to date to describe nuclear properties in the N=20 island of inversion. The comparison demonstrates the sensitivity of the low-lying excitation properties of the ^{29}Ne isotope to test and further improve these effective interactions. In particular, the important role of the neutron 3p4h configurations is pointed out for the N=19 odd-A isotopes near the drip line.

Declaration of competing interest

The authors declare that they have no known competing financial interests or personal relationships that could have appeared to influence the work reported in this paper.

Data availability

Data will be made available on request.

Acknowledgements

The authors would like to thank K. Wimmer for providing us the input for FRESCO calculations and A. Moro for giving access to an unpublished version of the FRESCO code.

This work was supported by the U.S. Department of Energy (DOE), Office of Science, Office of Nuclear Physics, under Grant No. DE-SC0020451, the U.S. National Science Foundation (NSF) under Grant No. PHY1565546 (Operation of the NSCL) and PHY2110365, and by the DOE National Nuclear Security Administration through the Nuclear Science and Security Consortium, under Award No. DE-NA0003180. GRETINA was funded by the DOE, Office of Science. Operation of the array at NSCL was supported by DOE under Grants No. DE-SC0019034 (NSCL) and No. DE-AC02-05CH11231 (LBNL). A.P. acknowledges the Grant CEX2020-001007-S funded by MCIN/AEI/10.13039/501100011033 and PGC-2018-94583. Y.U. and N.S. acknowledge KAKENHI Grant No. 20K03981 from the Ministry of Education, Culture, Sports, Science and Technology (MEXT), Japan. N.S. acknowledges support from “Program for Promoting Researches on the Supercomputer Fugaku” (JPMXP1020200105, hp210165, and hp220174) by JICFuS and MEXT, Japan. T.M. acknowledges the support by the Croatian Science Foundation under project No. IP-2018-01-1257.

References

[1] T. Otsuka, A. Gade, O. Sorlin, T. Suzuki, Y. Utsuno, Evolution of shell structure in exotic nuclei, Rev. Mod. Phys. 92 (2020) 015002, https://doi.org/10.1103/RevModPhys.92.015002.

[2] A. Poves, J. Retamosa, The onset of deformation at the N = 20 neutron shell closure far from stability, Phys. Lett. B 184 (4) (1987) 311–315, https://doi.org/10.1016/0370-2693(87)90171-7.

[3] E.K. Warburton, J.A. Becker, B.A. Brown, Mass systematics for A = 29 − 44 nuclei: the deformed A ∼ 32 region, Phys. Rev. C 41 (1990) 1147–1166, https://doi.org/10.1103/PhysRevC.41.1147.

[4] C. Thibault, et al., Direct measurement of the masses of ^{11}Li and $^{26-32}$Na with an on-line mass spectrometer, Phys. Rev. C 12 (1975) 644–657, https://doi.org/10.1103/PhysRevC.12.644.

[5] C. Détraz, et al., Mapping of the onset of a new region of deformation: the masses of ^{31}Mg and ^{32}Mg, Nucl. Phys. A 394 (3) (1983) 378–386, https://doi.org/10.1016/0375-9474(83)90111-2.

[6] N. Orr, et al., New mass measurements of neutron-rich nuclei near N = 20, Phys. Lett. B 258 (1) (1991) 29–34, https://doi.org/10.1016/0370-2693(91)91203-8.

[7] X. Zhou, et al., Direct mass measurements of the neutron-rich isotopes of fluorine through chlorine, Phys. Lett. B 260 (3) (1991) 285–290, https://doi.org/10.1016/0370-2693(91)91613-Z.

[8] F. Sarazin, et al., Shape coexistence and the N = 28 shell closure far from stability, Phys. Rev. Lett. 84 (2000) 5062–5065, https://doi.org/10.1103/PhysRevLett.84.5062.

[9] C. Détraz, et al., Beta decay of $^{27-32}$Na and their descendants, Phys. Rev. C 19 (1979) 164–176, https://doi.org/10.1103/PhysRevC.19.164.

[10] D. Guillemaud-Mueller, et al., β-decay schemes of very neutron-rich sodium isotopes and their descendants, Nucl. Phys. A 426 (1) (1984) 37–76, https://doi.org/10.1016/0375-9474(84)90064-2.

[11] T. Motobayashi, et al., Large deformation of the very neutron-rich nucleus ^{32}Mg from intermediate-energy Coulomb excitation, Phys. Lett. B 346 (1) (1995) 9–14, https://doi.org/10.1016/0370-2693(95)00012-A.

[12] Y. Yanagisawa, et al., The first excited state of ^{30}Ne studied by proton inelastic scattering in reversed kinematics, Phys. Lett. B 566 (1) (2003) 84–89, https://doi.org/10.1016/S0370-2693(03)00802-5.

[13] P. Doornenbal, et al., Mapping the deformation in the "island of inversion": inelastic scattering of ^{30}Ne and ^{36}Mg at intermediate energies, Phys. Rev. C 93 (2016) 044306, https://doi.org/10.1103/PhysRevC.93.044306.

[14] P. Doornenbal, et al., Spectroscopy of ^{32}Ne and the "island of inversion", Phys. Rev. Lett. 103 (2009) 032501, https://doi.org/10.1103/PhysRevLett.103.032501.

[15] B.V. Pritychenko, et al., First observation of an excited state in the neutron-rich nucleus ^{31}Na, Phys. Rev. C 63 (2000) 011305, https://doi.org/10.1103/PhysRevC.63.011305.

[16] B.V. Pritychenko, et al., Structure of the "island of inversion" nucleus ^{33}Mg, Phys. Rev. C 65 (2002) 061304, https://doi.org/10.1103/PhysRevC.65.061304.

[17] K. Yoneda, et al., Deformation of ^{34}Mg studied via in-beam γ-ray spectroscopy using radioactive-ion projectile fragmentation, Phys. Lett. B 499 (3) (2001) 233–237, https://doi.org/10.1016/S0370-2693(01)00025-9.

[18] H. Iwasaki, et al., Large collectivity of ^{34}Mg, Phys. Lett. B 522 (3) (2001) 227–232, https://doi.org/10.1016/S0370-2693(01)01244-8.

[19] A. Gade, et al., Spectroscopy of ^{36}Mg: interplay of normal and intruder configurations at the neutron-rich boundary of the "island of inversion", Phys. Rev. Lett. 99 (2007) 072502, https://doi.org/10.1103/PhysRevLett.99.072502.

[20] H.L. Crawford, et al., First spectroscopy of the near drip-line nucleus ^{40}Mg, Phys. Rev. Lett. 122 (2019) 052501, https://doi.org/10.1103/PhysRevLett.122.052501.

[21] E. Caurier, F. Nowacki, A. Poves, Merging of the islands of inversion at N = 20 and N = 28, Phys. Rev. C 90 (2014) 014302, https://doi.org/10.1103/PhysRevC.90.014302.

[22] N. Kobayashi, et al., One-neutron removal from ^{29}Ne: defining the lower limits of the island of inversion, Phys. Rev. C 93 (2016) 014613, https://doi.org/10.1103/PhysRevC.93.014613.

[23] T. Nakamura, et al., Deformation-driven p-wave halos at the drip line: ^{31}Ne, Phys. Rev. Lett. 112 (2014) 142501, https://doi.org/10.1103/PhysRevLett.112.142501.

[24] M. Takechi, et al., Interaction cross sections for Ne isotopes towards the island of inversion and halo structures of ^{29}Ne and ^{31}Ne, Phys. Lett. B 707 (3) (2012) 357–361, https://doi.org/10.1016/j.physletb.2011.12.028.

[25] C. Loelius, et al., Enhanced electric dipole strength for the weakly bound states in ^{27}Ne, Phys. Rev. Lett. 121 (2018) 262501, https://doi.org/10.1103/PhysRevLett.121.262501.

[26] J.G. Li, et al., One-neutron halo structure of ^{29}Ne, Phys. Lett. B 832 (2022) 137225, https://doi.org/10.1016/j.physletb.2022.137225.

[27] J. Chen, B. Singh, Nuclear data sheets for A = 33, Nucl. Data Sheets 112 (6) (2011) 1393–1511, https://doi.org/10.1016/j.nds.2011.04.003.

[28] C. Ouellet, B. Singh, Nuclear data sheets for A = 31, Nucl. Data Sheets 114 (2) (2013) 209–396, https://doi.org/10.1016/j.nds.2013.03.001.

[29] H.N. Liu, et al., Intruder configurations in the ground state of ^{30}Ne, Phys. Lett. B 767 (2017) 58–62, https://doi.org/10.1016/j.physletb.2017.01.052.

[30] M. Belleguic, et al., Search for neutron excitations across the N = 20 shell gap in $^{25-29}$Ne, Phys. Rev. C 72 (2005) 054316, https://doi.org/10.1103/PhysRevC.72.054316.

[31] E. Rodriguez-Vieitez, Structure and cross section data of neutron-rich N ∼ 20 nuclei produced in fragmentation and few-nucleon knockout reactions, Ph.D. thesis, University of California, Berkeley, 2017, https://publications.nscl.msu.edu/thesis/Rodriguez-Vieitez.

[32] H. Iwasaki, et al., Low-lying intruder 1^- state in ^{12}Be and the melting of the N = 8 shell closure, Phys. Lett. B 491 (1) (2000) 8–14, https://doi.org/10.1016/S0370-2693(00)01017-0.

[33] S. Paschalis, et al., The performance of the gamma-ray energy tracking in-beam nuclear array GRETINA, Nucl. Instrum. Methods Phys. Res., Sect. A 709 (2013) 44–55, https://doi.org/10.1016/j.nima.2013.01.009.

[34] D. Weisshaar, et al., The performance of the γ-ray tracking array GRETINA for γ-ray spectroscopy with fast beams of rare isotopes, Nucl. Instrum. Methods Phys. Res., Sect. A 847 (2017) 187–198, https://doi.org/10.1016/j.nima.2016.12.001.

[35] H. Iwasaki, et al., The TRIple PLunger for EXotic beams TRIPLEX for excited-state lifetime measurement studies on rare isotopes, Nucl. Instrum. Methods Phys. Res., Sect. A 806 (2016) 123–131, https://doi.org/10.1016/j.nima.2015.09.091.

[36] D. Bazin, et al., The S800 spectrograph, Nucl. Instrum. Methods Phys. Res., Sect. B 204 (2003) 629–633, https://doi.org/10.1016/S0168-583X(02)02142-0.

[37] D.J. Morrissey, et al., Commissioning the A1900 projectile fragment separator, Nucl. Instrum. Methods Phys. Res., Sect. B 204 (2003) 90–96, https://doi.org/10.1016/S0168-583X(02)01895-5.

[38] J. Yurkon, et al., Focal plane detector for the S800 high-resolution spectrometer, Nucl. Instrum. Methods Phys. Res., Sect. A 422 (1) (1999) 291–295, https://doi.org/10.1016/S0168-9002(98)00960-7.

[39] C. Loelius, Electromagnetic transition strengths studied with Doppler shift techniques across the contours of the valley of stability, Ph.D. thesis, Michigan State University, 2017, https://groups.nscl.msu.edu/nscl_library/Thesis/Loelius.

[40] S. Agostinelli, et al., Geant4 - a simulation toolkit, Nucl. Instrum. Methods Phys. Res., Sect. A 506 (3) (2003) 250–303, https://doi.org/10.1016/S0168-9002(03)01368-8.

[41] I.J. Thompson, Coupled reaction channels calculations in nuclear physics, Comput. Phys. Rep. 7 (4) (1988) 167–212, https://doi.org/10.1016/0167-7977(88)90005-6.

[42] A. Moro, private communication.

[43] K. Wimmer, et al., Shape coexistence revealed in the N = Z isotope ^{72}Kr through inelastic scattering, Eur. Phys. J. A 56 (6) (2020) 159, https://doi.org/10.1140/epja/s10050-020-00171-3.

[44] T. Furumoto, et al., Global optical potential for nucleus-nucleus systems from 50 MeV/u to 400 MeV/u, Phys. Rev. C 85 (2012) 044607, https://doi.org/10.1103/PhysRevC.85.044607.

[45] T. Furumoto, et al., Effect of repulsive and attractive three-body forces on nucleus-nucleus elastic scattering, Phys. Rev. C 80 (2009) 044614, https://doi.org/10.1103/PhysRevC.80.044614.

[46] T. Furumoto, et al., New complex G-matrix interactions derived from two- and three-body forces and application to proton-nucleus elastic scattering, Phys. Rev. C 78 (2008) 044610, https://doi.org/10.1103/PhysRevC.78.044610.

[47] J. Barrette, et al., Coulomb excitation of giant resonances in ^{208}Pb by E = 84MeV/Nucleon ^{17}O projectiles, Phys. Lett. B 209 (2) (1988) 182–186, https://doi.org/10.1016/0370-2693(88)90929-X.

[48] M. Fauerbach, et al., Coulomb excitation of the one-neutron halo nucleus ^{11}Be, Phys. Rev. C 56 (1997) R1–R4, https://doi.org/10.1103/PhysRevC.56.R1.

[49] T. Nakamura, et al., Halo structure of the island of inversion nucleus ^{31}Ne, Phys. Rev. Lett. 103 (2009) 262501, https://doi.org/10.1103/PhysRevLett.103.262501.

[50] B.V. Pritychenko, et al., Role of intruder configurations in ^{26,28}Ne and ^{30,32}Mg, Phys. Lett. B 461 (4) (1999) 322–328, https://doi.org/10.1016/S0370-2693(99)00850-3.

[51] V. Chisté, et al., Electric and nuclear transition strength in ^{30,32}Mg, Phys. Lett. B 514 (3) (2001) 233–239, https://doi.org/10.1016/S0370-2693(01)00796-1.

[52] J.A. Church, et al., Measurement of $e2$ transition strengths in ^{32,34}Mg, Phys. Rev. C 72 (2005) 054320, https://doi.org/10.1103/PhysRevC.72.054320.

[53] H. Mach, et al., New structure information on ^{30}Mg, ^{31}Mg and ^{32}Mg, Eur. Phys. J. A 25 (1) (2005) 105–109, https://doi.org/10.1140/epjad/i2005-06-159-0.

[54] K. Li, et al., Relativistic Coulomb excitation in ^{32}Mg near 200 MeV/nucleon with a thick target, Phys. Rev. C 92 (2015) 014608, https://doi.org/10.1103/PhysRevC.92.014608.

[55] R. Elder, et al., Lifetime measurements probing collectivity in the ground-state band of ^{32}Mg, Phys. Rev. C 104 (2021) 024307, https://doi.org/10.1103/PhysRevC.104.024307.

[56] C. Ouellet, B. Singh, Nuclear data sheets for A = 32, Nucl. Data Sheets 112 (9) (2011) 2199–2355, https://doi.org/10.1016/j.nds.2011.08.004.

[57] R.S. Lubna, et al., Structure of ^{38}Cl and the quest for a comprehensive shell model interaction, Phys. Rev. C 100 (2019) 034308, https://doi.org/10.1103/PhysRevC.100.034308.

[58] R.S. Lubna, et al., Evolution of the N = 20 and 28 shell gaps and two-particle-two-hole states in the FSU interaction, Phys. Rev. Res. 2 (2020) 043342, https://doi.org/10.1103/PhysRevResearch.2.043342.

[59] Y. Utsuno, et al., Varying shell gap and deformation in $n \sim 20$ unstable nuclei studied by the Monte Carlo shell model, Phys. Rev. C 60 (1999) 054315, https://doi.org/10.1103/PhysRevC.60.054315.

[60] S.M. Brown, et al., Low-lying neutron fp-shell intruder states in ^{27}Ne, Phys. Rev. C 85 (2012) 011302, https://doi.org/10.1103/PhysRevC.85.011302.
[61] N. Tsunoda, et al., Exotic neutron-rich medium-mass nuclei with realistic nuclear forces, Phys. Rev. C 95 (2017) 021304, https://doi.org/10.1103/PhysRevC.95.021304.
[62] F. Nowacki, A. Poves, New effective interaction for $0\hbar\omega$ shell-model calculations in the $sd-pf$ valence space, Phys. Rev. C 79 (2009) 014310, https://doi.org/10.1103/PhysRevC.79.014310.
[63] M. Holl, et al., Border of the island of inversion: unbound states in ^{29}Ne, Phys. Rev. C 105 (2022) 034301, https://doi.org/10.1103/PhysRevC.105.034301.
[64] H. Nishibata, et al., Structure of ^{31}Mg: shape coexistence revealed by $\beta-\gamma$ spectroscopy with spin-polarized ^{31}Na, Phys. Rev. C 99 (2019) 024322, https://doi.org/10.1103/PhysRevC.99.024322.